JOURNAL OF SOLID STATE CHEMISTRY 108, 284–290 (1994)

The Microstructure and Dielectric Properties of $Zr_5Ti_7O_{24}$ Ceramics

Feridoon Azough,* Andrew Wright,†,[1] and Robert Freer*,[2]

*Materials Science Centre, University of Manchester/UMIST, Grosvenor Street, Manchester M1 7HS, United Kingdom; and †Department of Chemistry, UMIST, P.O. Box 88, Sackville Street, Manchester M60 1QD, United Kingdom

Received December 10, 1992; accepted June 1, 1993.

Ceramics of $Zr_5Ti_7O_{24}$ have been prepared by the mixed oxide route. Specimens sintered at 1400°C were at 95% of theoretical density. Transmission electron microscopy (TEM) electron diffraction studies established the existence of a one-dimensional superlattice in the *a*-direction. Computer generated TEM images and electron diffraction patterns aided the interpretation of experimental diffraction patterns and lattice images. At 5 GHz the relative permittivity was 34.1 and the dielectric *Q* value 700. Such low *Q* values are attributed to the presence of the sintering aid Y_2O_3, which is necessary for the formation of $Zr_5Ti_7O_{24}$.

INTRODUCTION

Zirconium titanate-based ceramics are temperature stable dielectics (1) that find practical applications as resonators at microwave frequencies (2). The end member $ZrTiO_4$ has an orthorhombic structure (3, 4) of the α-PbO_2 type, space group *Pbcn, with cell edges* $c > b > a$. However, the length of the longest cell edge is sensitive to processing conditions. McHale and Roth (5, 6) demonstrated that zirconium titanate specimens sintered at approximately 1500°C and annealed at temperatures as low as 900°C had *c* cell parameters in the range 0.5483 to 0.5348 nm, with most of the change occurring for specimens annealed between 1100 and 1190°C. This led to the description of zirconium titanate in terms of a high temperature form (long *c* cell edge) and a low temperature form (short *c* cell edge) with the transition at 1175 ± 10°C (5, 6). Such behavior was attributed to ordering of cations within the α-PbO_2 structure, the high temperature form being fully disordered and the low temperature form exhibiting a significant degree of ordering.

Neutron diffraction studies by Bordet *et al.* (7) supported the model of high temperature zirconium titanate as a disordered structure and indicated that the compound $Zr_5Ti_7O_{24}$ had an ordered superstructure of the α-PbO_2 type.

Preliminary transmission electron microscopy (TEM) electron diffraction and lattice imaging studies by Azough and Freer (8) of zirconium titanate ceramics cooled at different rates after sintering showed a change from a disordered to an incommensurate superlattice structure.

Recent high resolution TEM studies by Christoffersen and Davies (9) of a single crystal and a powder having compositions in the system $ZrTiO_4$–$Zr_5Ti_7O_{24}$ confirmed the presence of an incommensurate superstructure for compositions with Zr : Ti between 5 : 7 and 1 : 1, while phases close to 1 : 1 had a commensurate superstructure with a doubled *a*-axis.

Azough and Freer (10, 11) found that zirconium titanate (ZT) and $Zr_{0.8}Sn_{0.2}TiO_4$ (ZTS) ceramics sintered at 1400°C and cooled at different rates (water quench, air quench, . . . , 1°C/hr) exhibited a wide range of electrical properties. The dielectric *Q* values for ZTS specimens at 5 GHz decreased from 10,200 for ceramics cooled at 1°C/hr to 3000 for air quenched specimens (11). ZT specimens also show such changes (10). Hirano *et al.* (12) noted a correlation between the cell parameters for ZT and ZTS specimens and their dielectric *Q* values. Samples with shorter cell parameters along the *c*-axis (higher degrees of ordering) exhibited higher *Q* values. High resolution transmission electron microscope studies by the present authors (10, 13) confirmed major changes in the microstructures for both ZT and ZTS ceramics, with the development of a superstructure in the *a*-direction in the more slowly cooled specimens.

Cation ordering in zirconium titanate-based ceramics therefore appears to have a significant effect on the gross microstructure (in terms of the length of the *c*-cell edge) and local microstructure which affects the electrical properties. Since $Zr_5Ti_7O_{24}$ has been proposed as the ideal fully ordered form of zirconium titanate (7, 11), it is desirable to understand the behavior and the properties of $Zr_5Ti_7O_{24}$ and its relationship with the family of zirconium titanate

[1] Present address: Advanced Materials Research Laboratory, Multidisciplinary Research and Innovation Centre (MRIC), The North East Wales Institute (NEWI), Kelsterton Road, Connah's Quay, Clwyd CH5 4BR, United Kingdom.

[2] To whom correspondence should be addressed.

0022-4596/94 $6.00

materials. The present investigation is part of a continuing study of zirconium titanate-based ceramics and considers both the microstructure and dielectric properties of $Zr_5Ti_7O_{24}$ ceramics. Specimens have been prepared by the mixed oxide route, and in accordance with earlier studies (6, 7) it has been necessary to employ a small amount of Y_2O_3 in order to develop the $Zr_5Ti_7O_{24}$ structure.

EXPERIMENTAL

1. Materials and Preparation

The starting materials were ZrO_2 (Magnesium Electron, MEL E20 grade), TiO_2 (Tioxide A-HR), ZnO (BDH chemicals analar grade), and Y_2O_3 (Fluka, analar grade). The oxides in the desired proportions (i.e., to give Zr/Ti = 5/7, plus 1 wt% Y_2O_3 and 1.5 wt% ZnO) were wet mixed for 8 hr, calcined at 1100°C for 4 hr, and milled again for 12 hr. Pellets were pressed at 120 MPa in the shape of discs 16 mm in diameter and 8 mm high. Sintering was performed at 1400°C for 4 hr in air. The heating rate was 180°C/hr and the cooling rate was 6°C/hr.

2. Characterization of Powders and Products

X-ray diffraction analysis, using Cu$K\alpha$ radiation and a Philips diffractometer with horizontal goniometer, was employed to examine calcined powders and sintered specimens. Product morphologies and microstructures were examined by optical microscopy (on polished surfaces and etched surfaces); by scanning electron microscopy, using Philips 505 and 525 instruments (on polished and fractured surfaces); and by transmission electron microscopy.

Samples for TEM studies were prepared by grinding crushed pellets in an agate mortar and pestle and then depositing particles on a carbon-coated copper grid. A Philips EM430 Transmission Electron Microscopy was used for lattice image and electron diffraction studies. Lattice images were obtained at an accelerating voltage of 300 keV by the Many Beam Imaging (MBI) method. The electron beam was parallel to [011] orientation and the selected objective aperture contained both the fundamental and the superlattice reflections.

In order to interpret the high resolution images in terms of the projected structure, image simulations were performed using the multislice method (14), as implemented in the VISP program suite (15). The structure model of Bordet *et al.* (7) was used to generate phase gratings of 256 × 64 points using Fourier coefficients out to 6 $Å^{-1}$. Slice thicknesses of 0.5 Å were used in the multislice interation and the effects of inelastic scattering were not considered. Images were calculated from the diffraction

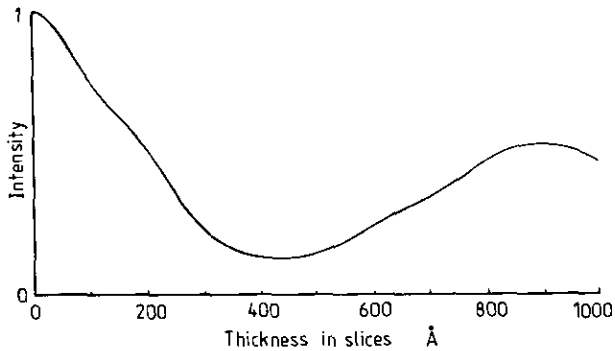

FIG. 1. The intensity of zero order (transmitted beam) as a function of crystal thickness.

space wavefield using the full nonlinear (partially coherent illumination) model (14).

Images were simulated at two crystal thicknesses: first for a crystal of 7.3 Å thickness (strong phase object) and then for a crystal of 880 Å thickness. The thickness of 7.3 Å corresponds to *one* repeat in the [011] direction (i.e., $\sqrt{2} \times 5.4$). This is the minimum crystal thickness which may reasonably be expected to occur in practice. Simulation at 880 Å thickness was performed because at this crystal thickness, a maximum in the zero order (000) beam occurs. At this condition a bright thickness fringe appears in cleaved wedges of crystal fragments, as shown in Fig. 1. (Thus it is possible to fix one of the two main variables, defocus and crystal thickness, needed as input to the simulation program). The range of defocus used for the two crystal thicknesses was 0.0 Å (Gaussian) to −1050 Å (under focus) in 50 Å steps. The effects of using partially coherent illumination were simulated using a beam convergence of 0.5 milliradians and a spread of 130 Å root mean square (rms). Projected crystal structures were generated using the STRUPLO84 package (16).

Dielectric properties at 1 kHz and temperatures in the range 25 to 120°C were determined for 3 mm thick polished discs (bearing Ag electrodes) using a Wayne Kerr 6425 precision component analyzer in conjunction with a dedicated sample cell.

High frequency dielectric measurement were performed at 5 GHz (25°C) on polished discs (13 mm in diameter, 7 mm high), with a network analyzer and sweep oscillator (the Hakki and Coleman method (17)).

RESULTS AND DISCUSSION

Calcined powders were white in color with an average grain size of 2.8 μm. X-ray diffraction analysis of the powders indicated formation of the compound $Zr_5Ti_7O_{24}$, with minor amounts of unreacted ZrO_2 and TiO_2.

Sintered products were white-cream in color and ap-

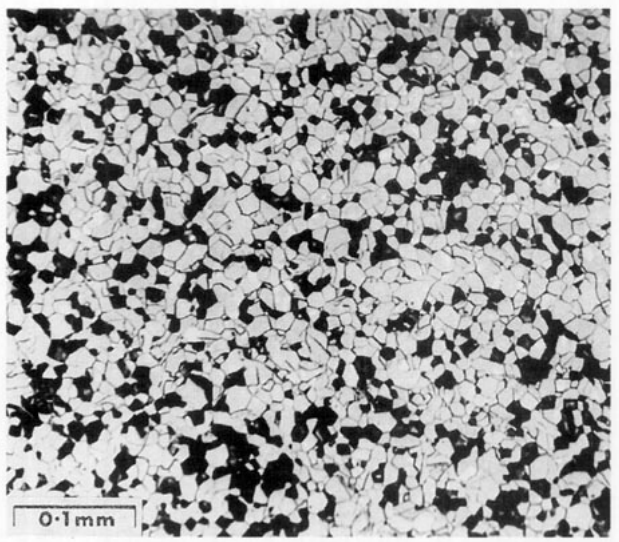

FIG. 2. Optical micrograph of $Zr_5Ti_7O_{24}$ ceramic (prepared with 1.5 wt% ZnO and 1.0 wt% Y_2O_3).

TABLE 1
X-ray Diffraction Data for Sintered $Zr_5Ti_7O_{24}$ Ceramic Samples (2θ = 10° to 100°)

d(Å)	hkl	I/I_0	d(Å)	hkl	I/I_0
3.5523	130	13	1.6790	330	6
2.8987	131	100	1.6677	311	6
2.6627	200	15	1.5829	113	9
2.5504	141	2	1.5154	133	8
2.5040	002	10	1.4647	082	8
2.4652	012	2	1.4542	262	6
2.3902	060	5	1.4185	203	2
2.3532	201	4	1.4126	213	2
2.2190	032	2	1.3906	332	3
2.1328	240	3	1.2911	371	2
2.1118	231	7	1.1995	124	3
2.051	042	4	1.1964	012	2
1.8266	202	13	1.1909	390	2
1.8102	212	2	1.1831	134,372	2
1.7819	260	13	1.1670	460	2
1.6979	261	2	1.1585	391	3
			1.1373	461	3

proximately 95% of theoretical density. X-ray analysis showed only single phase $Zr_5Ti_7O_{24}$. Figure 2 shows an optical micrograph of a polished and etched specimen. The texture was soft, as shown by the degree of grain pull-out, with an average grain size of 12 μm. Grain shape was predominantly euhedral, but occasionally angular.

The addition of ZnO promoted densification and led to the formation of a (Zn–Ti)-rich phase, of approximate formula Zn_2TiO_4, at the grain boundaries.

The presence of a small quantity of Y_2O_3 appears to be necessary for the formation of $Zr_5Ti_7O_{24}$. Yttria could not, however, be detected in the grain boundaries or second phase, and is therefore believed to be incorporated within the primary phase. This is in accordance with the findings of McHale and Roth (5). To a first approximation the composition of the matrix may be regarded as $Zr_5Ti_7O_{24}$, and for the purpose of description this formula is employed for the remainder of this discussion.

X-ray diffraction data for the ceramic are listed in Table 1. The d-spacings and intensities are in excellent agreement with published data (18), except that diffraction lines with d-spacings of 7.1873, 3.5428, and 3.2573 Å were absent from our patterns.

On the assumption of an orthorhombic crystal structure, the cell parameters were calculated to be a = 14.353 Å, b = 5.325 Å, and c = 5.016 Å. These values are very close to the results obtained by Bordet *et al.* (7) by neutron diffraction techniques.

TEM electron diffraction studies confirmed the existence of a one dimensional superlattice in the a-direction. Figure 3 shows an [011] electron diffraction pattern of $Zr_5Ti_7O_{24}$. The length of the unit cell of the fundamental lattice in the a-direction is approximately 4.8 Å; the unit cell of the superstructure is three times larger, approximately 14.4 Å, in agreement with the X-ray data.

Figure 4 is a TEM image (with electron beam parallel to [011]) showing the 14.4 Å superlattice which corresponds to the spacing of (100) planes. Irregular broad dark fringes can also be seen crossing parallel to the (100) fringes. These can be interpreted as antiphase boundaries. A high resolution magnified TEM image of one of these boundary regions is shown in Fig. 5. This reveals a shift in the fringe position across the boundary. This fringe

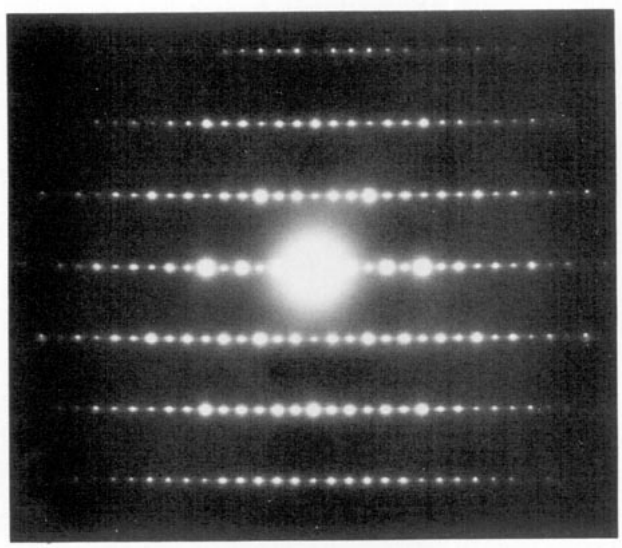

FIG. 3. [011] electron diffraction pattern for $Zr_5Ti_7O_{24}$.

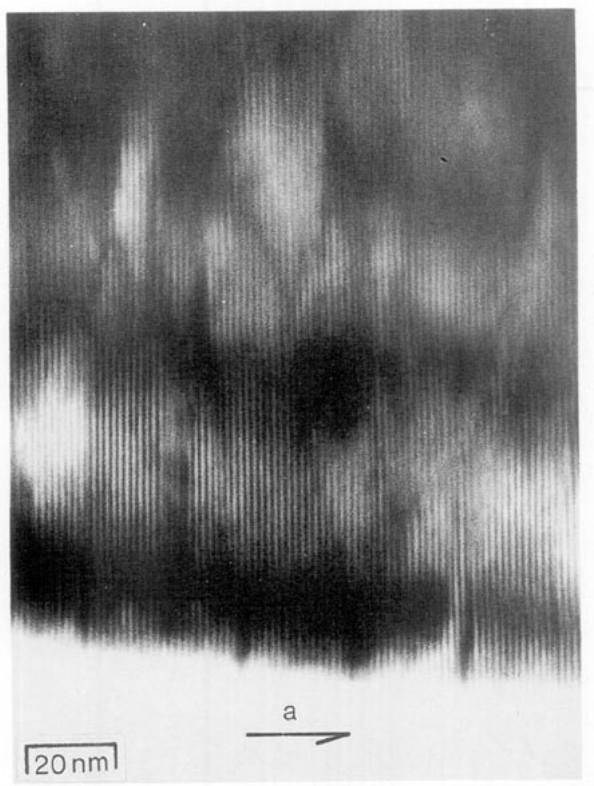

FIG. 4. TEM image of the $Zr_5Ti_7O_{24}$ structure (electron beam parallel to [011]).

shift is typical of HRTEM images of antiphase boundaries and has been seen in many structure types (e.g., lead magnesium niobate (19), $Pb(Mg_{1/3}Nb_{2/3})O_3$, and lead scandium tantalate (20), $Pb(Sc_{1/2}Ta_{1/2})O_3$).

Figure 6 is a high resolution, high magnification lattice image of the ceramic, with the electron beam parallel to [011]. This shows the lattice image of $Zr_5Ti_7O_{24}$ in more detail.

A projected potential of $Zr_5Ti_7O_{24}$ along the [011] direction is shown in Fig. 7. Greater insight is gained from a projection for the structure in terms of atom positions (Fig. 8) which was obtained via the STRUPLO84 program. The unit cell of the superstructure for $Zr_5Ti_7O_{24}$ is outlined in Fig. 8. Ordering structure are discussed in some detail by Christoffersen and Davis. (9).

Figures 9a and 9b show computer simulated electron microscope images as a function of defocus of the objective lens for slice thicknesses of 7.3 and 880 Å, respectively. The generated images for a thin crystal (Fig. 9a) may be compared with the projected potential (Fig. 7); this shows that the black "atoms" occur over the focus range of −400 to −900 Å. Outside this range, the contrast is reversed. Experimentally, the defocus was adjusted close to the Scherzer setting (−735 Å for this instrument). This was achieved via knowledge of both the step size (6 nm) and the number of steps away from minimum contrast at the specimen edge. It should be noted that minimum contrast of the amorphous material at the specimen edge does not correspond to zero defocus but to a slight under focus. This value can be calculated if the objective lens parameters are known. For this instrument, the correction factor is −243 Å. Thus setting the objective lens to the Scherzer condition ensures that, for a weak phase object such as a very thin crystal, the dark contrast corresponds to "black" atom columns. The edge of the crystal seen in the experimental image in Fig. 6 appears to be sufficiently thin to match well with the simulations in this focus and thickness regime. Simulations produced using a crystal thickness of 880 Å (Fig. 9b), which show no direct correspondence with the projected potential, do match well with thicker regions (right hand side of Fig. 6). Any change in the amount of defocus between matches for the thin crystal and thick crystal can be explained in

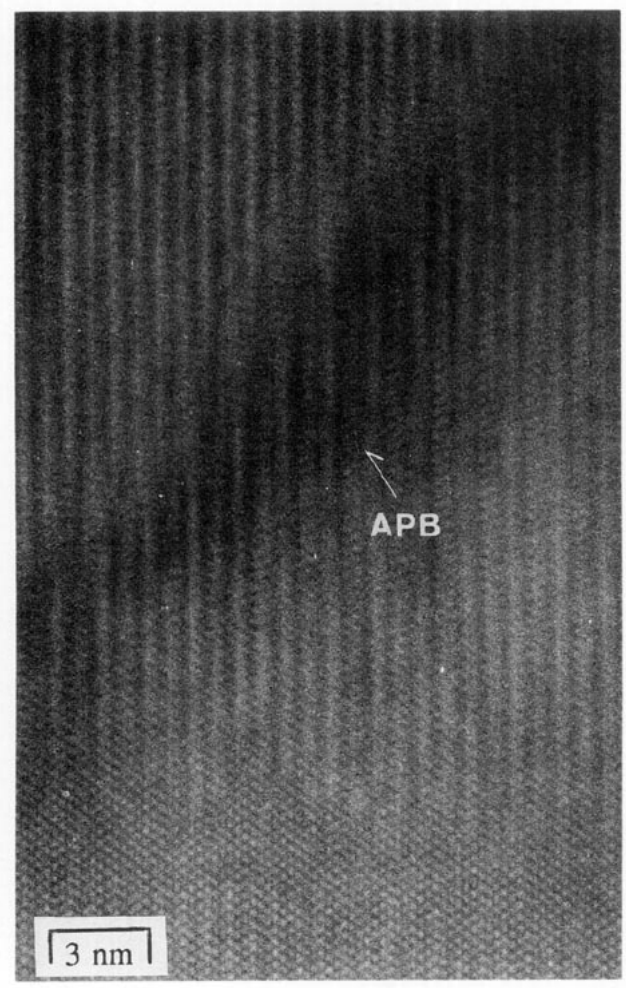

FIG. 5. High resolution electron microscope lattice image of $Zr_5Ti_7O_{24}$, showing an antiphase domain boundary (APB).

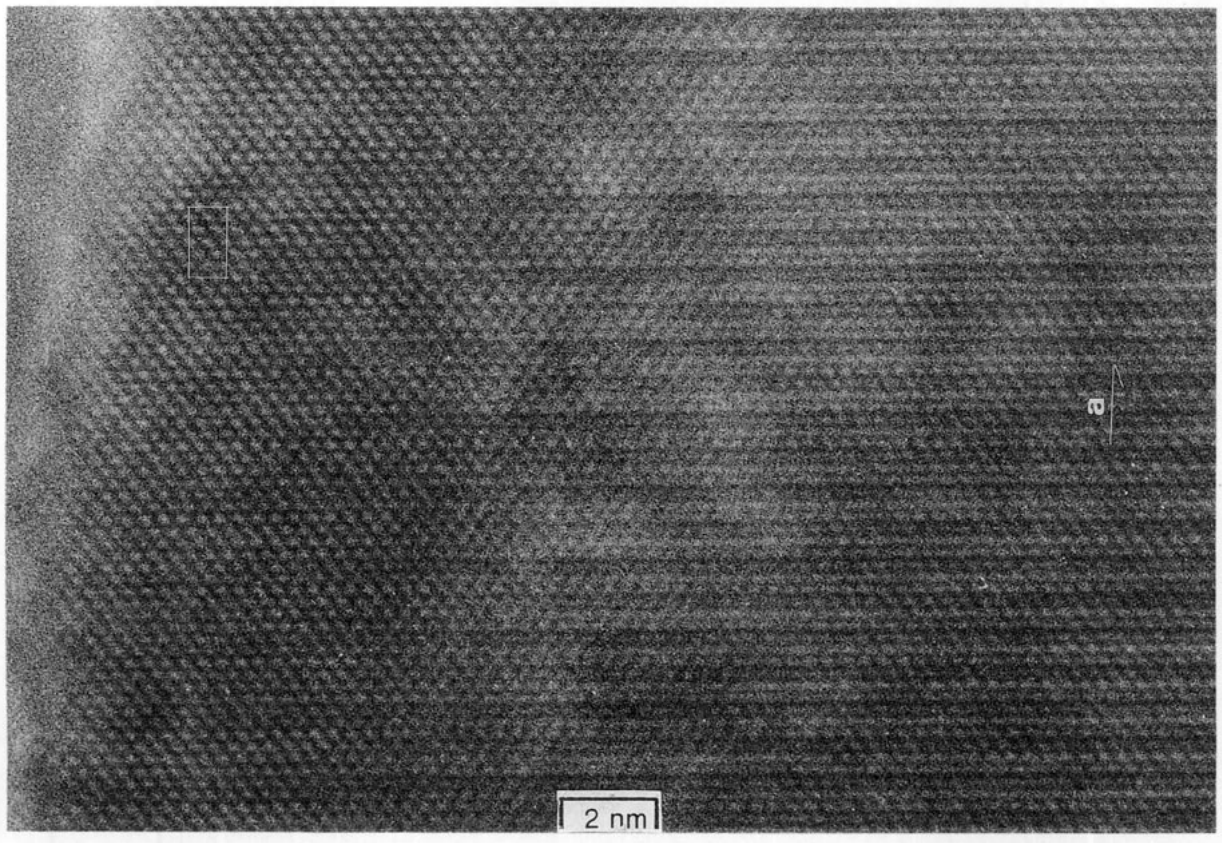

FIG. 6. High resolution electron microscope lattice image of $Zr_5Ti_7O_{24}$ (at higher magnification than Fig. 5). Electron beam is parallel to [011]. The unit cell is outlined. The sample increases in thickness from left to right across the figure.

terms of an inclined crystal fragment. Exact matches for thicker crystals are difficult to obtain due to the effects of the crystal misalignment and the neglect of inelastic scattering effects.

The results obtained from the current TEM investigation of $Zr_5Ti_7O_{24}$ ceramics confirmed the structure proposed by Bordet *et al.* (7) with cations ordered in the *a*-direction, giving a superstructure with a tripled *a*-axis.

The dielectric properties of the $Zr_5Ti_7O_{24}$ ceramic are summarized in Table 2. The low frequency relative permittivity (ε_r) and Q values of $Zr_5Ti_7O_{24}$ are lower than those reported (8) for $ZrTiO_4$ (i.e., $\varepsilon_r = Q = 1000$ at 1 kHz) and the temperature coeffcient of capacitance (τ_c) is higher than that for $ZrTiO_4$ ($\tau_c = 110$ ppm/°C at 1 kHz).

At 5 GHz the Q-value of $Zr_5Ti_7O_{24}$ was only 700. It is believed that this does not represent the intrinsic Q value of the pure material and that the presence of Y^{3+} ions in the $Zr_5Ti_7O_{24}$ has degraded the dielectric properties. In

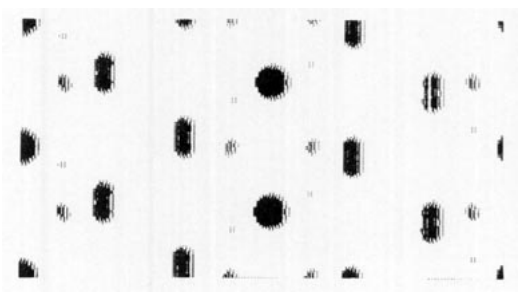

FIG. 7. Projected potential for $Zr_5Ti_7O_{24}$ along [011].

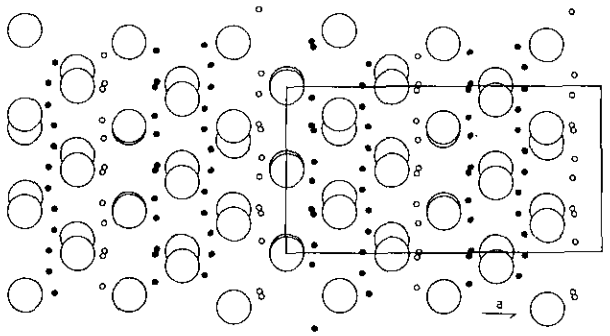

FIG. 8. [011] Projection showing the atomic positions in $Zr_5Ti_7O_{24}$. Within the unit cell (outlined) the large circles are oxygen atoms, small black circles are Ti atoms and small open circles are Zr atoms.

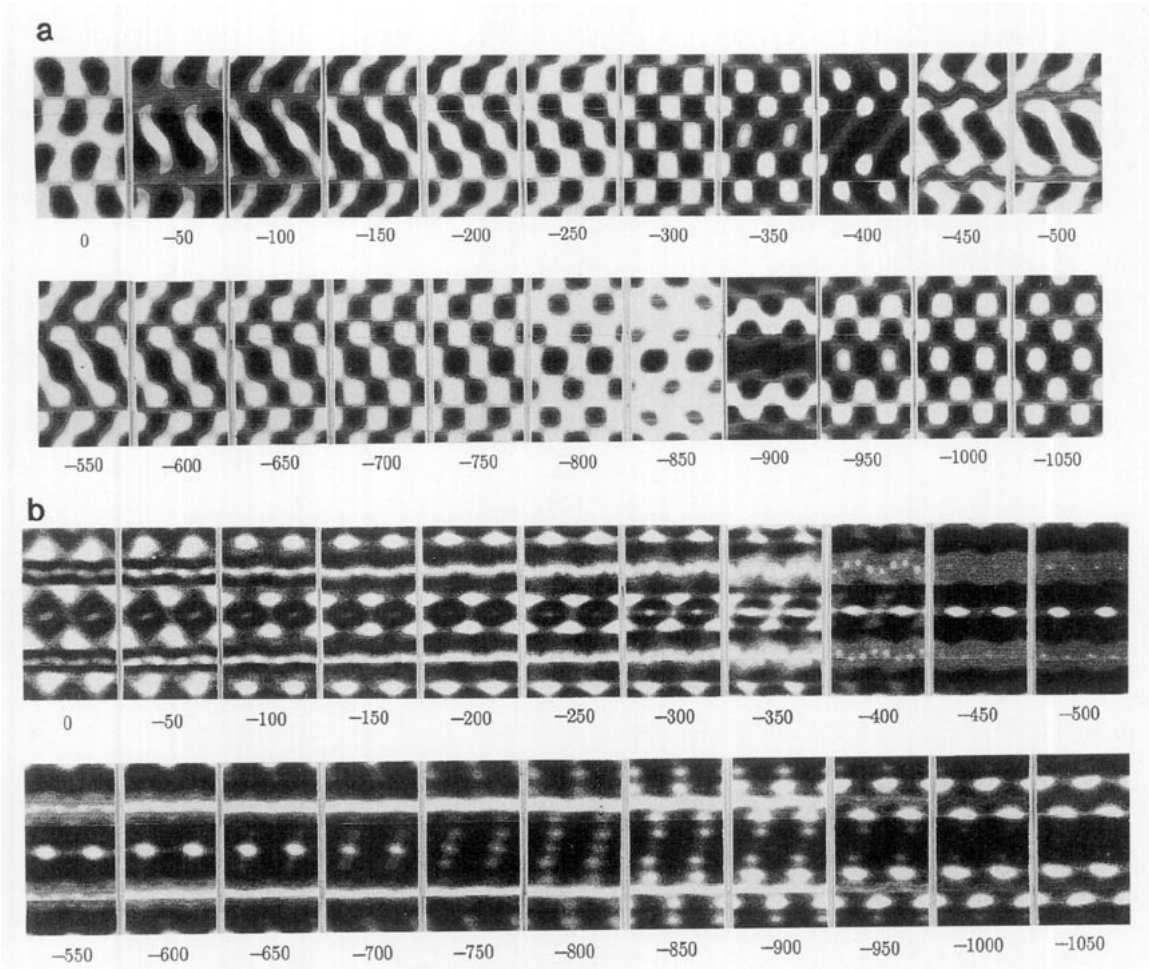

FIG. 9. Computer simulated TEM images of $Zr_5Ti_7O_{24}$ as a function of the defocus of the objective lens for (a) a slice thickness of 7.3 Å, and (b) a slice thickness of 880 Å.

related studies of $ZrTiO_4$ ceramics (10), specimens doped with Y_2O_3 again showed reduced Q values, as low as 500, while ceramics free of Y_2O_3 had Q-values of 4000–4500 at 5 GHz (Table 3).

The degradation of the dielectric Q values of zirconium titanate-based ceramics by the introduction of elements of valency 3, such as Fe^{+3}, La^{+3}, and Cr^{+3}, has been reported by several authors (24–26). In each case the trivalent elements appear to diffuse into host grains. Wakino *et al.* (24) noted that the deleterious effect of Fe^{+3} could be overcome if NiO was also added to help form a Ni–Fe–Ti rich grain boundary phase, thereby preventing Fe^{+3} from entering the host grains. For example, ZTS ceramics containing 0.5% Fe_2O_3 had a dielectric Q value at 7 GHz of 400, but the addition of 0.5% NiO enabled the Q value to be increased to 5000. The paradox in the case of $Zr_5Ti_7O_{24}$ ceramics is that while the Y^{3+} almost certainly contributes to a lowering of the Q value, there

TABLE 2
Dielectric Properties of $Zr_5Ti_7O_{24}$ Ceramics

Frequency	ε_r	Q value	τ_c (ppm/°C)
1 kHz	35.9	660	160*
5 GHz	34.1	700	—

* (20 − 120°C)

TABLE 3
Microwave Dielectric Properties of $ZrTiO_4$ Ceramics

Frequency	ε_r	Q value	ref
7 GHz	42	4000	(21)
2.2 Ghz	42	9000	(22)
6 GHz	39	3700	(23)
5 GHz	40–41	4000–4500	(8)

appears to be no easy way to prepare $Zr_5Ti_7O_{24}$ ceramics without the addition of a small amount of yttria. In principle, it is possible that Y^{3+} could substitute for Zr^{4+} and/or Ti^{4+} and simultaneously create oxygen vacancies. In such a case the presence of oxygen vacancies may lead to a lowering of the Q value. From the pale color of the specimens it would appear that the $Zr_5Ti_7O_{24}$ ceramics did not contain a significant fraction of oxygen vacancies. However, the defect concentration could not be formally quantified using the techniques employed in this study.

Further experiments are now needed to define the role of Y^{3+} and its effect on lowering the dielectric Q value of $Zr_5Ti_7O_{24}$ ceramics.

CONCLUSIONS

Zirconium-deficient Zirconium titanate, $Zr_5Ti_7O_{24}$, has an orthohombic crystal structure, where the cell parameter in the a-direction is approximately three times longer than that in the high temperature form of $ZrTiO_4$. The presence of the superstructure was confirmed by electron diffraction studies.

Simulation of TEM images using the multislice method enabled theoretical images to be generated for different crystal thicknesses. Good agreement was obtained with experimental lattice images for selected focus conditions.

The relative permittivities and dielectric Q values of $Zr_5Ti_7O_{24}$ were lower than anticipated. The fact that the Q values for $Zr_5Ti_7O_{24}$ were less than 800 at 5 GHz appears to be due to the presence of the additive Y_2O_3, which was employed to ensure the formation of the $Zr_5Ti_7O_{24}$ structure.

REFERENCES

1. W. Rath, *Keram, Rundschau* **49,** 137 (1941).
2. K. Wakino, *in* "Proceedings of the Sixth IEEE International Symposium on Applications of Ferroelectrics, Lehigh University," p. 97. 1986.
3. R. E. Newnham, *J. Am. Ceram. Soc.* **50,** 216 (1967).
4. R. W. Lynch and B. Morosin, *J. Am. Ceram. Soc.* **55,** 409 (1972).
5. A. E. McHale and R. S. Roth, *J. Am. Ceram. Soc.* **66,** C18 (1983).
6. A. E. McHale and R. S. Roth, *J. Am. Ceram. Soc.* **69,** 827 (1986).
7. P. Bordet, A. E. McHale, A. Santaro, and R. S.Roth, *J. Solid State Chem.* **64,** 30 (1986).
8. F. Azough and R. Freer, *in* "Euro-Ceramics, Proceedings of the 1st European Ceramic Society Meeting, Maastricht, 1989" (G. de With, R. A. Terpistra, and R. Metselaar Eds.), Vol. 2, p. 290. Elsevier Applied Science, London/New York, 1989.
9. R. Christoffersen and P. K. Davies, *J. Am. Ceram. Soc.* **75,** 563, (1992).
10. F. Azough, Ph.D. Thesis. University of Manchester, 1991.
11. F. Azough and R. Freer, *in* "Proceedings of the Seventh IEEE International Symposium on Applications of Ferroelectrics, University of Illinois at Urbana–Champaign, 1990" p. 198. 1991.
12. S. Hirano, T. Hayashi, and A. Hattori, *J. Am. Ceram. Soc.* **74,** 1320 (1991).
13. F. Azough, I. Brough, P. Kenway, R. Freer, and G. W. Lorimer, *in* "Proceedings of the Institute of Physics Electron Microscopy and Analysis Group and Royal Microscopical Society Conference, EMAG-MICRO 89" (P. Goodhew and H. Elder, Eds.), Institute of Physics Conference Series No. 98, p. 431. 1990.
14. K. Ishizaka and N. Uyeda, *Acta Crystallogr. Sect. A* **33,** 740 (1979).
15. A. C. Wright, unpublished work.
16. R. X. Fisher, *J. Appl. Crystallogr.* **18,** 258 (1985).
17. B. W. Hakki and P. D. Coleman, *IRE Trans. Microwave Theory Technol.* **MTT-8,** 402 (1960).
18. JCPDS File, No. 34-209.
19. J. Chen, H. M. Chan, and M. P. Harmer, *J. Am. Ceram. Soc.***72,** 593 (1989).
20. K. Z. Baba-Kishi, I. M. Reaney, and D. J. Barber, *J. Mater. Sci.* **25,** 1645 (1990).
21. H. Ouchi and S. Kawashima, *Jpn. J. Appl. Phys.* **24,** Supplement 24-2, 60 (1985).
22. G. Wolfram and H. E. Gobel, *Mater. Res. Bull.* **16,** 1455 (1981).
23. P. C. Osbond, R. W. Whatmore, and F. W. Ainger, *Br. Ceram. Proc.* **36,** 167 (1985).
24. K. Wakino, K. Minai, and H. Tamua,*J. Am. Ceram. Soc.* **67,** 278 (1984).
25. D. M. Iddles, A. J., Bell, and A. J. Moulson, *in* "Proceedings of the 1st European Ceramic Society Conference, Maastricht, 1989" (G. de With, R. A. Terpstra, and R. Metselaar, Eds.), Vol. 2, p. 166. Elsevier Applied Science, London/New York, 1989).
26. F. Azough and R. Freer, *Br. Ceram. Proc.* **42,** 225 (1989).